IEEE Access
Multidisciplinary ⋮ Rapid Review ⋮ Open Access Journal

Received January 7, 2018, accepted February 6, 2018, date of publication February 12, 2018, date of current version May 24, 2018.

Digital Object Identifier 10.1109/ACCESS.2018.2805384

Locating an Acoustic Emission Source in Multilayered Media Based on the Refraction Path Method

ZILONG ZHOU, YICHAO RUI, JING ZHOU, LONGJUN DONG, (Member, IEEE), AND XIN CAI
School of Resources and Safety Engineering, Central South University, Changsha 410083, China

Corresponding author: Yichao Rui (ruiyichao@csu.edu.cn)

This work was supported in part by the National Basic Research Program of China (973 Program) under Grant 2015CB060200 and in part by the National Natural Science Foundation of China under Grant 41772313 and Grant 51478479.

ABSTRACT The traditional acoustic emission (AE) source location method, which is based on the model of a single-layered medium, is not appropriate for accurately locating AE sources in multilayered media. To solve this problem, an innovative AE source location method based on a refraction path (RP) method is proposed. In this new method, the refraction points at each interface are first solved according to Snell's law and then substituted into the equations for the time difference of arrival (TDOA). Second, linear equations can be obtained by linearizing the TDOA equations. Finally, the optimal AE source can be obtained by iteratively updating the trial solution based on the linearized equations. The results of a pencil-lead break experiment and a numerical simulation show that the proposed method is applicable of locating the actual AE source in both the single- and multilayered media, and the location error of this method in multilayered media is significantly smaller than that of the traditional method.

INDEX TERMS Acoustic emission, source location, multilayered media, refraction path, time difference of arrival.

I. INTRODUCTION

Acoustic emission (AE), which is important for nondestructive testing techniques, is extensively used to monitor structural integrity and to study material damage mechanisms [1]–[7]. A primary and fundamental step in analyzing acoustic emissions is to identify the location of damage, providing more valuable information beyond simply the presence of damage [8]–[12]. Therefore, a highly accurate method for locating the AE source has continuously been a prime research interest [13]–[18].

Many AE source location methods have been developed and widely implemented in various applications, which mainly include analytical and iterative methods [19], [20]. The basic thought of the analytical methods is to obtain the explicit formulas for AE source through the nonlinear governing equations [21]–[24]. For the iterative methods, most of them were developed from Geiger method [25]–[28] that converted the nonlinear governing equations into linear by using a first order Taylor expansion. These traditional methods are mainly based on the assumption of homogeneous and isotropic, where the straight-line paths between the source and AE sensors are considered. However, the media encountered in engineering practice usually are more complex [29]–[35], which have multiple layers, or interlayers between the AE source and sensors [36]. Therefore, neglecting the refractions by these traditional methods though assuming straight-line paths can introduce significant errors to the source location results [37].

To solve the problem of source location for complex medium, Gollob *et al.* [38] presented the FastWay method by using the minimum travel-time path. Prasanna *et al.* [39] took minimum energy path to obtain a practicable source location solution in a more general setup on any arbitrary surface containing finite discontinuities. Both two methods can locate the AE sources in heterogeneities and geometrical irregularities of foreknown material properties. Nevertheless, two methods have either heavy computing burden or the results are not ideal because of the heavy dependency on the voxel or grid partition. Furthermore, some signal-based source localization methods, such as time reversal methods have recently been introduced by Ing *et al.* [40] and Ribay *et al.* [41], which can achieve the source location in complex media as well. The advantage is that they do not require the knowledge of the wavespeed or the structural geometry. However, they

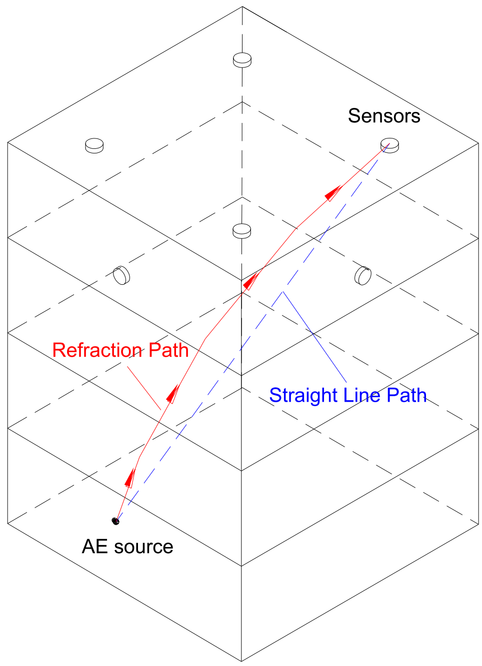

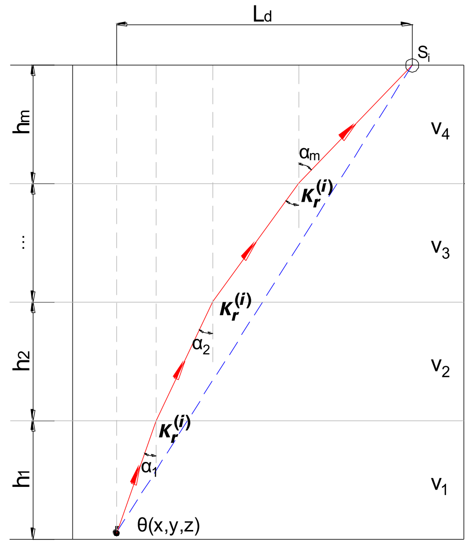

FIGURE 1. **Schematic of the AE wave propagation path: (a) spatial paths considering and disregarding refraction and (b) sectional view of the AE wave paths. $\alpha_1, \alpha_2, \cdots, \alpha_M$ are the incidence angles or the angles of refraction on each interface. $K_r^{(i)}$ is the refraction points with the coordinates $(x_r^{(i)}, y_r^{(i)}, z_r^{(i)})$ at the i^{th} RP. $v_1, v_2, \cdots v_m$ and $h_1, h_2, \cdots h_m$ are the propagation speeds of the acoustic waves and heights of each medium layer, respectively.**

require repeated training, which can take a long time to cover the whole area. Then, Park *et al.* [42] improved this method by automatic training in which noncontact scanning laser Doppler vibrometer and the existing piezoelectric transducers were applied. For more complex structures having circular holes on the path between the acoustic source and the sensor, Baxter *et al.* [43] and Hensman *et al.* [44] proposed the Delta-T method to improve source location by comparing differences in the time of arrival information for each sensor pair between a training data set and an actual impact event [45]–[47]. The above time reversal methods can solve the source location in complex structures and can also be applied in layered media. But they are labor intensive and computationally demanding due to the requirement of training data in advance. Therefore, the specific research for the source location with a stronger computing power in the layered media will be necessary. Hence, Zhang *et al.* [48] simplified the travel time equation utilizing the approximate refraction points in linear equations for the location of layered medium. Their method is efficient but the approximate refraction points may cause large location errors. Therefore, the combined forward and inversion method was further proposed [49], which had higher location accuracy. However, it is not suitable for the condition where sensors are far away from the hypocenter. In 2017, Zhou *et al.* [50] proposed an AE source location method for different media based on Snell's law, which resulted in smaller location errors in layered media than traditional methods. However, they only located the AE in media with two layers.

To accurately and efficiently locate AE sources in multilayered media, the refraction path (RP) location method is proposed. The location errors of the new method and traditional method are analyzed and compared.

II. THE RP LOCATION METHOD

A. PRINCIPLE OF THE RP METHOD

In traditional AE location methods, objects containing AE sources are treated as single-layered media, assuming the acoustic wave propagates along the blue dashed line in Fig. 1(a), and the mixed wave velocity is used in the arrival time equations:

$$t_i^s = t_0 + \frac{L^{(i)}}{\bar{v}} \tag{1}$$

where t_i^s is the arrival time of an AE event at the i^{th} $(i = 1, 2, \cdots, N)$ sensor. t_0 is the initial time of the AE event, and $\bar{v}$ is the mixed velocity. (x_i, y_i, z_i) are the coordinates of the i^{th} sensor, and θ is the AE source with coordinates (x, y, z). $L^{(i)}$ is the straight-line distance between the AE source and sensor i, and $L^{(i)} = \sqrt{(x-x_i)^2 + (y-y_i)^2 + (z-z_i)^2}$.

However, when the measured objects have multiple layers, the AE signal will be refracted at the interfaces of the different layers during propagation. The RPs are represented by red solid lines in Fig. 1(a). The arrival time of this RP can be expressed as:

$$t_i = t_0 + \sum_{m=1}^{M_i} \frac{L_m^{(i)}}{v_m} \tag{2}$$

where t_i is the arrival time obtained by the i^{th} ($i = 1, 2, \cdots, N$) sensor under the RP model, v_m is the speed in the m^{th} layer, $m = 1, 2 \cdots, M_i$, and L_m is the length of the propagation path in the m^{th} layer. In the expression for L_m, $\left(x_r^{(i)}, y_r^{(i)}, z_r^{(i)}\right)$ are the coordinates of the refraction point on the r^{th} ($r = 1, 2 \cdots, M_i - 1$) interface for the i^{th} propagation path.

$$L_m^{(i)} = \begin{cases} \sqrt{(x - x_r^{(i)})^2 + (y - y_r^{(i)})^2 + (z - z_r^{(i)})^2}, \\ \quad m = 1, \quad r = 1 \\ \sqrt{(x_r^{(i)} - x_{r-1}^{(i)})^2 + (y_r^{(i)} - y_{r-1}^{(i)})^2 + (z_r^{(i)} - z_{r-1}^{(i)})^2}, \\ \quad 1 < m \le M_i - 1, \quad r = m \\ \sqrt{(x_i - x_r^{(i)})^2 + (y_i - y_r^{(i)})^2 + (z_i - z_r^{(i)})^2}, \\ \quad m = M_i, \quad r = M_i - 1 \end{cases}$$

Sensor 1 is assumed to be the first to detect the acoustic wave. By subtracting the equation for $i = 1$ from the equation for $i > 1$, the initial time t_0 can be eliminated, and the time difference of arrival (TDOA) equation can be obtained:

$$\Delta t_{i1} = t_i - t_1 = \sum_{m=1}^{M_i} \frac{L_m^{(i)} - L_m^{(1)}}{v_m} \tag{3}$$

where M_i is the layer on which the i^{th} AE sensor is placed. If the AE sensors are mounted on different layers, M_i will be different. If AE sensors are on the same layer, M_i will be the same. After knowing which layer the i^{th} AE sensor is located on, the refraction points at each interface for i^{th} refraction path (RP) can be solved according to Snell's law and then are substituted into (3).

B. DETERMINATION OF REFRACTION POINTS

In (3), the unknowns that must be further determined are the source coordinates (x, y, z) and the coordinates $x_r^{(i)}$ and $y_r^{(i)}$ of the refraction points. Meanwhile, the refraction of an acoustic wave at interfaces in multilayered media should also meet Snell's law [51], as shown in Fig. 1(b). Their relations can be represented as (4)

$$\frac{\sin \alpha_m}{U_m} = B^{(i)}, \quad m = 1, 2, \cdots, M_i \tag{4}$$

where $U_m = v_m / v_{\max}$, $v_{\max} = \max(v_1, v_2, \cdots, v_m)$, and $B^{(i)}$ is a constant under the i^{th} propagation path. The constant falls between 0 and 1.

The horizontal distance between the AE source and sensor i is $L_h^{(i)}$, which satisfies the following relations:

$$L_h^{(i)} = \sum_{m=1}^{M_i} h_m \tan \alpha_m \tag{5}$$

where $\tan \alpha_m = \frac{\sin \alpha_m}{\sqrt{1 - \sin^2 \alpha_m}}$, and $L_h^{(i)} = \sqrt{(x_i - x)^2 + (y_i - y)^2}$.

The only unknown, $B^{(i)}$, can be rapidly calculated by substituting (4) into (5). Then, $\tan \alpha_m$ can be obtained according to the solution of $B^{(i)}$. Finally, the coordinates of the refraction points on each interface can be obtained:

$$[x_r^{(i)}, y_r^{(i)}] = \begin{cases} [x, y] + \vec{e}_i h_1 \tan \alpha_m, & r = 1, \ m = 1 \\ [x_{r-1}^{(i)}, y_{r-1}^{(i)}] + \vec{e}_i h_m \tan \alpha_m, & r > 1, \ m > 1 \end{cases} \tag{6}$$

where $\vec{e}_i = [x_i - x, y_i - y] / \sqrt{(x_i - x)^2 + (y_i - y)^2}$, which is the direction vector of the straight-line projection of the propagation path onto the x-y plane.

C. SOLUTION PROCEDURE FOR THE RP METHOD

The residual functions expressing the deviations between the calculated and observed TDOA can then be obtained with the following expression:

$$\xi_i(\theta) = \Delta t_{i1}^c - \Delta t_{i1}^o \tag{7}$$

where the deviation ξ is called the TDOA residual error. The smaller the deviation is, the closer the test point is to the true AE source. In addition, Δt_{i1}^c is the calculated TDOA between sensor i ($i = 2, 3, \cdots, N$) and sensor 1, and Δt_{i1}^o is the observed TDOAs at sensor i and sensor 1.

The unknown parameters $\theta\,(x, y, z)$ can be obtained by solving (7), but the nonlinear equations are difficult to solve directly. Therefore, we adopt the iteration method to solve the nonlinear equations. In each iteration step, the parameter vector θ is replaced by a new estimate $(\theta + \Delta\theta)$. To determine $\Delta\theta$, the functions are approximated by their linearizations (i.e., the TDOA equations are linearized using a first-order Taylor expansion):

$$\xi_i(\theta) = \frac{\partial \Delta t_{i1}}{\partial x} \Delta x + \frac{\partial \Delta t_{i1}}{\partial y} \Delta y + \frac{\partial \Delta t_{i1}}{\partial z} \Delta z, \quad i = 2, 3, \cdots, N \tag{8}$$

For N sensors, there are $N - 1$ equations, and (8) can be written as a matrix:

$$A \Delta\theta = \gamma \tag{9}$$

where

$$A = \begin{bmatrix} \frac{\partial \Delta t_{21}}{\partial x} & \frac{\partial \Delta t_{21}}{\partial y} & \frac{\partial \Delta t_{21}}{\partial z} \\ \frac{\partial \Delta t_{31}}{\partial x} & \frac{\partial \Delta t_{31}}{\partial y} & \frac{\partial \Delta t_{31}}{\partial z} \\ \vdots & \vdots & \vdots \\ \frac{\partial \Delta t_{N1}}{\partial x} & \frac{\partial \Delta t_{N1}}{\partial y} & \frac{\partial \Delta t_{N1}}{\partial z} \end{bmatrix},$$

$$\Delta\theta = \begin{bmatrix} \Delta x \\ \Delta y \\ \Delta z \end{bmatrix}, \quad \gamma = \begin{bmatrix} \xi_2 \\ \xi_3 \\ \vdots \\ \xi_i \end{bmatrix}$$

$$\frac{\partial \Delta t_{i1}}{\partial x} = \frac{(x - x_i)}{v_1 L_1^{(i)}} - \frac{(x - x_1)}{v_1 L_1^{(1)}}, \quad \frac{\partial \Delta t_{i1}}{\partial y} = \frac{(y - y_i)}{v_1 L_1^{(i)}} - \frac{(y - y_1)}{v_1 L_1^{(1)}},$$

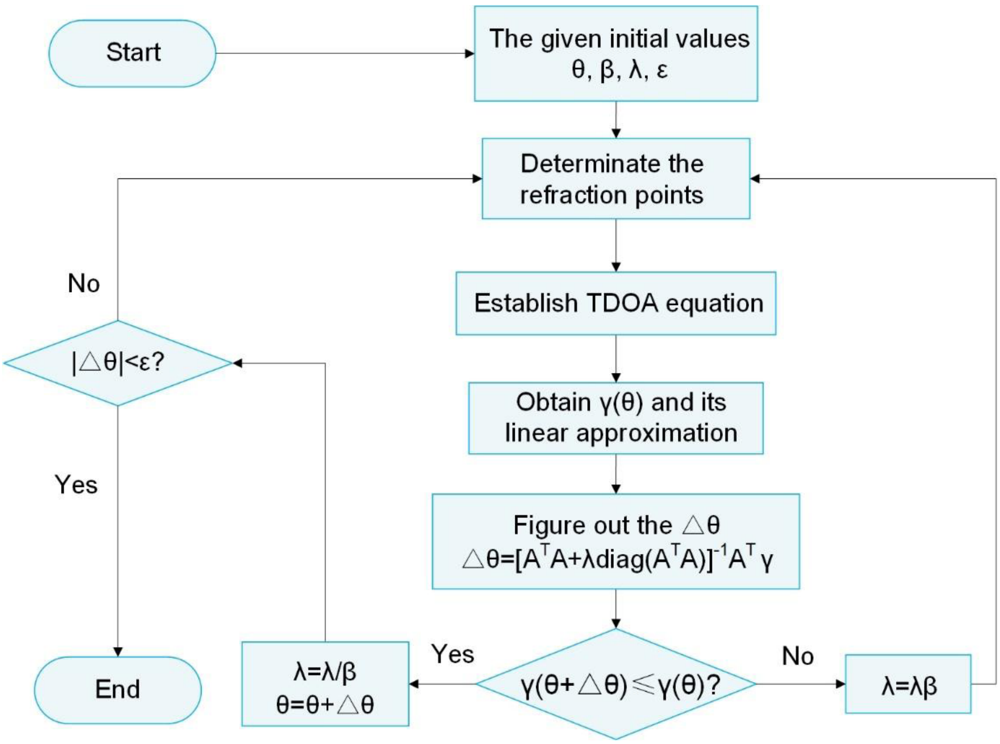

FIGURE 2. Flowchart of the RP method.

and

$$\frac{\partial \Delta t_{i1}}{\partial z} = \frac{(z - z_i)}{v_1 L_1^{(i)}} - \frac{(z - z_1)}{v_1 L_1^{(1)}}.$$

The least squares solution defined by (9) satisfies

$$A^T A \Delta\theta = A^T \gamma \tag{10}$$

or

$$\Delta\theta = \left(A^T A\right)^{-1} A^T \gamma$$

where the symbol T denotes the matrix transpose, and $A^T A$ is the Hessian matrix.

However, when the initial value is distant from the true solution, the first-order approximation of the Taylor expansion will easily lead to the singularity of the Hessian matrix, which makes inverting the matrix in (10) difficult, and the iteration will be terminated. To solve this problem, a damping term $\lambda\text{diag}(A^T A)$ is added to the Hessian matrix, which enables the iteration to continue [27], [52], and (10) becomes

$$[A^T A + \lambda diag(A^T A)]\Delta\theta = A^T \gamma \tag{11}$$

or

$$\Delta\theta = [A^T A + \lambda diag(A^T A)]^{-1} A^T \gamma$$

where λ is a nonnegative damping factor that is adjusted in each iteration. If the reduction in the residual error is rapid, a smaller value ($\lambda = \lambda/\beta$) can be used, bringing the algorithm closer to the Gauss–Newton algorithm. Where, the constant β is the control factor of the step size with a value $\beta > 1$. If an iteration results in an insufficient reduction in the residual, λ can be increased ($\lambda = \beta\lambda$), moving a step closer to the gradient-descent direction. If either the length of the calculated step $\Delta\theta$ or the reduction in the residual sum of squares from the latest parameter vector $\theta + \Delta\theta$ falls below predefined limits, the iteration stops, and the last parameter vector θ is considered the solution. Diagonal matrix diag($A^T A$) consists of the diagonal elements of $A^T A$. Each component of the gradient can be scaled according to the diagonal elements of $A^T A$, thus providing some advantages of the second derivative even for large λ. The diagonal matrix will ensure that movements will be larger along the directions where the gradients are smaller. This avoids slow convergences in the directions of small gradients.

The entire process of the RP method is shown in detail in Fig. 2.

III. EXPERIMENTAL VERIFICATION

To verify the feasibility of this method, an AE source location experiment was carried out in multilayered media. Three different materials were selected, iron, granite and marble. The AE sources were generated by breaking pencil lead. The diameter of the HB pencil lead was 0.5 mm, and the pencil lead was broken at 30ř on the surfaces of the specimens.

Fig. 3 shows the locations of the AE sources and sensors in the experiment. The bottom layer was a marble specimen with a velocity $v_1 = 5007$m/s. The middle layer was a granite specimen with $v_2 = 4442$m/s. The top layer was an iron

TABLE 1. The location results of the pencil-lead break experiment.

Location	Sources	True coordinates (mm)			Calculated AE sources coordinates (mm)						Absolute distance error (mm)	
					RP			TD				
		x	y	z	x	y	z	x	y	z	RP	TD
Top layer	T_1	0	120	214	0	119.2	215.1	0	119.2	215.1	2.2	2.2
	T_2	0	60	199	0.3	59.4	200	0.3	59.4	200	1.6	1.6
	T_3	70	0	184	69.1	0	183.1	69.1	0	183.1	1.7	1.7
	T_4	140	0	169	140.3	0	168.4	140.3	0	168.4	0.9	0.9
Middle layer	Q_1	0	120	130	0.5	119.3	131.3	13.3	114.7	149.3	3.8	23.9
	Q_2	0	60	115	0.0	58.9	114.1	11.2	61.6	143.8	1.8	30.9
	Q_3	70	0	100	70.4	0.0	103.5	74.1	8.2	139.0	3.7	40
	Q_4	140	0	85	139.9	2.7	86.7	134.8	13.1	131.2	4.8	48.3
Bottom layer	P_1	0	120	55	0.9	119.6	59.9	19.3	111.0	122.1	5.2	68.5
	P_2	0	60	40	1.3	60.4	38.9	17.4	64.2	106.5	7.7	70.7
	P_3	70	0	25	71.1	0.1	26.3	77.1	13.2	97.9	6.8	72.5
	P_4	140	0	10	139.0	2.2	14.7	131.1	17.1	91.5	5.7	83.5

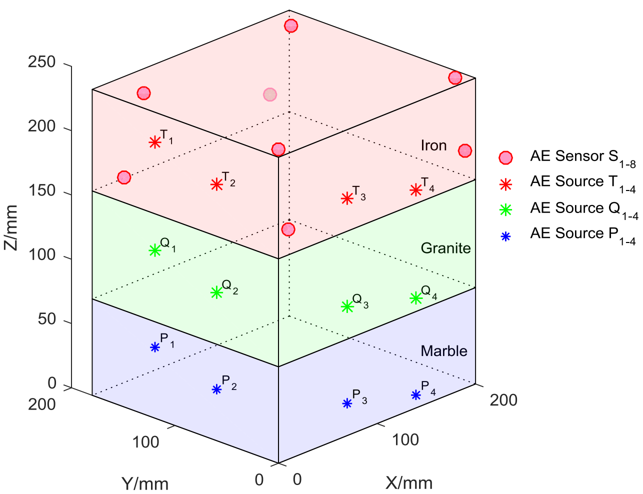

FIGURE 3. Locations of the AE sources and sensors.

specimen with $v_3 = 6047$m/s. The three specimens had the same lengths and widths (200 mm×179 mm), and the heights of the marble, granite and iron layers were 75, 84, and 79 mm, respectively. Eight AE sensors were placed on the surface of the top layer at the following coordinates: S_1 (0, 149, 179), S_2 (10, 0, 179), S_3 (200, 10, 179), S_4 (180, 179, 179), S_5 (20, 149, 238), S_6 (10, 10, 238), S_7 (190, 10, 238), and S_8 (180, 159, 238). It should be noted that the AE sensors have not to be placed in the same layer, they can be mounted on different layers as long as the engineering practice permits. But in the paper, the AE sensors were all mounted in the top layer in order to get closer to specific engineering practices, e.g., in the mining monitoring system where the majority of sensors are placed on or in the superficial layer. And another case is the true triaxial test where the AE sensors are difficult to be mounted on the surface of rock sample directly. Four AE sources were generated by breaking pencil leads on each layer. The coordinates of the AE sources are listed in Table 1.

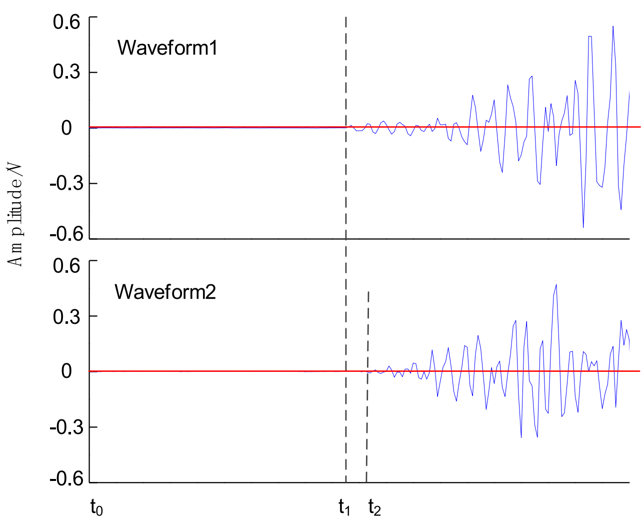

FIGURE 4. AE signals and arrival times at different sensors.

The AE waveforms received at two sensors are shown in Fig. 4, and t_1 and t_2 are the arrival times at sensor 1 and sensor 2. The AE sources were located by using the proposed RP method and the traditional TD method [28].

The locations determined using the two methods and their projections onto three planes' coordinates are plotted in three-dimensional space in Fig. 5. The location results in the top

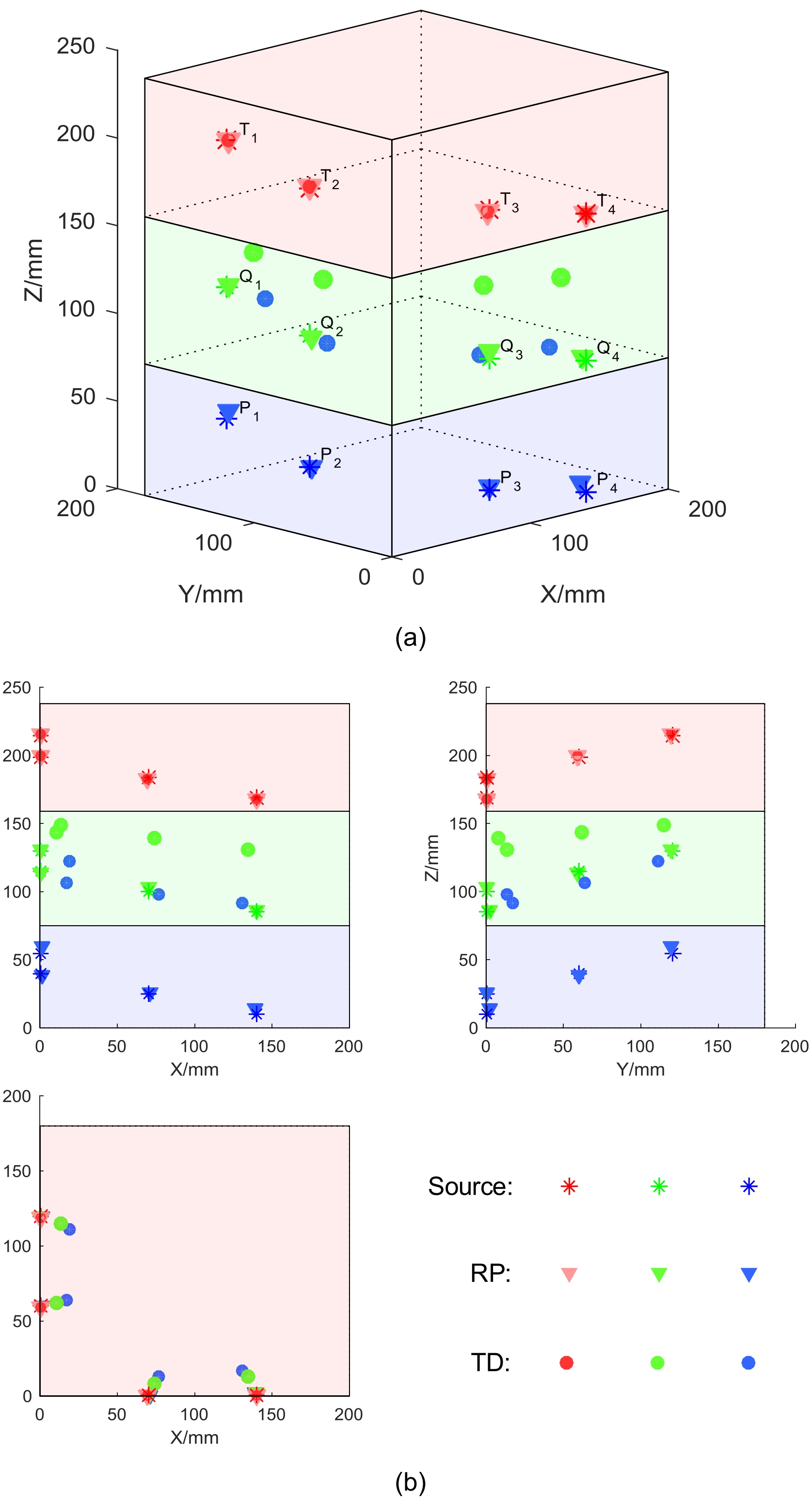

FIGURE 5. Location results from the two methods: (a) 3D schematic diagram of the location results; (b) Projections of AE events on the x-z, y-z, and x-y planes.

medium using the two methods are unanimous because there was no refraction. In the middle layer, the advantage of the RP method is clear, and the locating errors from the RP method are much smaller than those from TD. The location results from the two methods differ most in the bottom layer; the TD method locate the AE sources in the middle

TABLE 2. AE source coordinates determined using the two methods.

Media Layer	Methods	Coordinates of AE sources (mm)											
		A_i			B_i			C_i			D_i		
		x	y	z	x	y	z	x	y	z	x	y	z
1 layer	Source	100.00	220.00	805.00	80.00	80.00	825.00	220.00	80.00	845.00	200.00	200.00	865.00
	RP	100.07	220.00	804.97	79.96	80.03	824.86	219.96	80.04	844.92	200.01	199.94	865.06
	TD	100.07	220.00	804.97	79.96	80.03	824.86	219.96	80.04	844.92	200.01	199.94	865.06
3 layers	Source	100.00	220.00	645.00	80.00	80.00	665.00	220.00	80.00	685.00	200.00	200.00	705.00
	RP	100.07	219.97	644.85	79.91	80.06	665.17	219.92	79.94	684.92	200.16	200.06	704.85
	TD	104.77	213.99	601.39	86.54	82.26	609.04	213.00	81.90	631.95	193.09	197.53	669.09
5 layers	Source	100.00	220.00	485.00	80.00	80.00	505.00	220.00	80.00	525.00	200.00	200.00	545.00
	RP	100.11	219.83	484.94	80.06	79.86	505.39	219.91	80.21	525.70	200.02	199.99	545.06
	TD	103.02	216.20	386.57	82.01	79.78	392.40	218.14	79.83	419.68	197.60	199.73	456.67
7 layers	Source	100.00	220.00	325.00	80.00	80.00	345.00	220.00	80.00	365.00	200.00	200.00	385.00
	RP	99.88	220.12	324.93	79.97	80.10	345.38	220.14	80.09	364.38	200.42	200.11	383.69
	TD	102.22	217.22	141.72	80.75	79.38	143.58	219.49	79.15	173.04	199.15	200.45	213.02
9 layers	Source	100.00	220.00	165.00	80.00	80.00	185.00	220.00	80.00	205.00	200.00	200.00	225.00
	RP	100.43	219.52	166.50	80.17	80.31	186.51	220.37	79.50	202.71	200.15	200.05	224.44
	TD	102.49	216.99	-131.13	80.46	79.29	-135.79	220.19	78.29	-107.81	199.38	200.67	-59.67
11 layers	Source	100.00	220.00	5.00	80.00	80.00	25.00	220.00	80.00	45.00	200.00	200.00	65.00
	RP	100.07	219.85	4.00	79.95	79.99	24.29	219.97	79.77	43.03	200.08	200.05	65.46
	TD	101.96	217.53	-443.29	79.97	78.80	-454.37	220.02	78.43	-417.73	199.59	200.83	-363.91

layer, whereas the location errors when using the RP method remain small. Therefore, the proposed method is more applicable for determining locations in multi-layer media. Table 1 lists the location results from the RP and traditional methods.

IV. SIMULATION AND ANALYSIS

The above experiment shows that the RP method can accurately locate AE sources in multilayered media. The characteristics of the RP method using simulated AE source locations is analyzed in this section.

The simulation is based on an 11-layer media model, in which the dimensions of each layer are 300 mm × 300 mm × 80 mm. Sixteen sensors are deployed in the top medium at the following coordinates: O_1 (10, 300, 810), O_2 (0, 10, 820), O_3 (300, 0, 810), O_4 (300, 300, 820), O_5 (0, 135, 810), O_6 (145, 0, 820), O_7 (300, 155, 810), O_8 (165, 300, 820), O_9 (0, 300, 880), O_{10} (0, 0, 880), O_{11} (300, 0, 880), O_{12} (300, 300, 880), O_{13} (0, 135, 880), O_{14} (140, 0, 880), O_{15} (300, 155, 880), and O_{16} (165, 300, 880) (in mm). From the bottom up, the velocities of the layer media uniformly varied from 6000 m/s to 3000 m/s. Four different AE sources denoted by A, B, C, and D are located in the different layers at the coordinates listed in Table 2. The AE sources in each layer can be located using the proposed RP method based on the simulated times of arrival (the precision is 10^{-7} s), sensor locations and velocities. The results obtained using the RP and TD methods, which are presented in detail in Table 2, are compared.

Fig. 6 shows the trends of the absolute distance errors of the two methods for different source locations in the layers. The RP method has a small theoretical locating error, and the four curves almost completely overlap. Meanwhile, the TD method has larger location errors for the multilayered media, which increase significantly from the top to the bottom layer. As there is no refraction in the single layer, the location

TABLE 3. Absolute distance errors of the locations determined using the two methods.

Method	AE sources	Absolute distance error (mm)					
		1 layer	3 layers	5 layers	7 layers	9 layers	11 layers
RP	A_i	0.08	0.17	0.21	0.18	1.63	1.01
	B_i	0.15	0.20	0.42	0.40	1.55	0.71
	C_i	0.10	0.13	0.74	0.64	2.37	1.99
	D_i	0.08	0.23	0.07	1.37	0.58	0.48
Mean Error		0.10	0.18	0.36	0.65	1.53	1.05
TD	A_i	0.08	44.28	98.55	183.31	296.16	448.30
	B_i	0.15	56.38	112.62	201.42	320.79	479.37
	C_i	0.10	53.54	105.34	191.97	312.82	462.73
	D_i	0.08	36.65	88.37	171.99	284.67	428.91
Mean Error		0.10	47.71	101.22	187.17	303.61	454.83

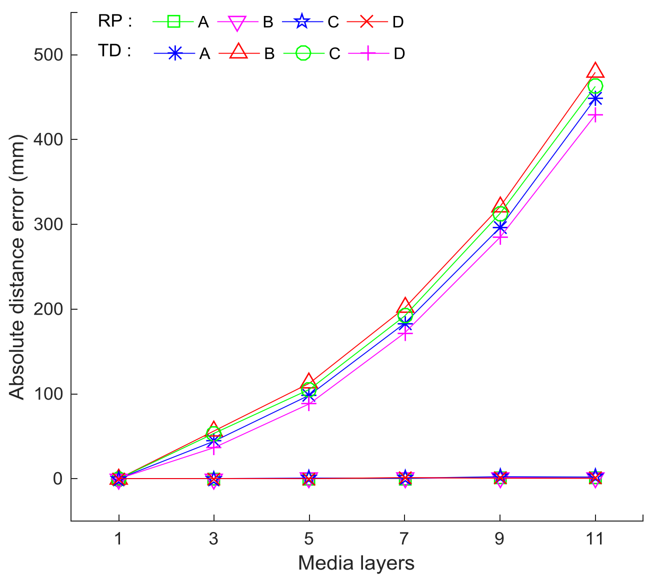

FIGURE 6. Relationships between absolute distance error and the number of media layers.

errors of the two methods exactly coincide. Detailed data are presented in Table 3.

V. CONCLUSIONS

This paper proposes an AE source location method for multilayered media that assumes that acoustic waves spread along a straight line in a single layer and will refract at the interface between different layers. In this method, the determination of the refraction points is convenient and rapid because the equation contains only one unknown parameter. In addition, the amount of calculations for the refraction points does not considerably increase with number of layers. For the iteration process, a damping term is added to the Hessian matrix, which avoids the singularity of the matrix and enables iterations to continue successfully, even for inaccurate initial values. Rapid convergence using the RP method can be achieved by adjusting the damping factor. The pencil-lead break experiment shows that the RP method is applicable to locating AE sources in both single and multilayered media. The proposed method is more accurate than the traditional TD method in multilayered media. Furthermore, the numerical simulation demonstrates the stability of the RP method in location performance. The theoretical location error under the RP method is small, whereas the absolute distance error under the TD method increases significantly with layers.

However, the proposed algorithm has some limitations. First, this location method can be applied only to multilayered structures of isotropic non-dispersive layers of known geometry and layer-to-layer interfaces, whereas many media have more sophisticated structures such as the media with arbitrary shaped interfaces which can be further investigated combining the theory of minimum energy path or others [39]. Second, the velocity in each layer must be measured in advance. Therefore, operational errors in velocities may occur, which would lead to errors in the final AE source locations. Moreover, note that location accuracy is also related to sensor layout, but their specific relationships require further research. Therefore, future studies should extend this method to overcome those limitations.

REFERENCES

[1] M. Strantza, D. Van Hemelrijck, P. Guillaume, and D. G. Aggelis, "Acoustic emission monitoring of crack propagation in additively manufactured and conventional titanium components," *Mech. Res. Commun.*, vol. 84, pp. 8–13, Sep. 2017.

[2] D. G. Aggelis, T. Shiotani, S. Momoki, and A. Hirama, "Acoustic emission and ultrasound for damage characterization of concrete elements," *ACI Mater. J.*, vol. 106, no. 6, pp. 1–6, Nov. 2009.

[3] K. Ohno and M. Ohtsu, "Crack classification in concrete based on acoustic emission," *Construction Building Mater.*, vol. 24, no. 12, pp. 2339–2346, Dec. 2010.

[4] S. Yin, S. X. Ding, X. Xie, and H. Luo, "A review on basic data-driven approaches for industrial process monitoring," *IEEE Trans. Ind. Electron.*, vol. 61, no. 11, pp. 6418–6428, Nov. 2014.

[5] F. Grigoli *et al.*, "Automated microseismic event location using master-event waveform stacking," *Sci. Rep.*, vol. 6, May 2016, Art. no. 25744.
[6] A. Behnia, H. K. Chai, and T. Shiotani, "Advanced structural health monitoring of concrete structures with the aid of acoustic emission," *Construction Building Mater.*, vol. 65, pp. 282–302, Aug. 2014.
[7] Y. Ling and S. Mahadevan, "Integration of structural health monitoring and fatigue damage prognosis," *Mech. Syst. Signal Process.*, vol. 28, no. 19, pp. 89–104, Apr. 2012.
[8] S. Xu, J. P. Liu, S. D. Xu, J. Wei, W. B. Huang, and L. B. Dong, "Experimental studies on pillar failure characteristics based on acoustic emission location technique," *Trans. Nonferrous Metals Soc. China*, vol. 22, no. 11, pp. 2792–2798, Nov. 2012.
[9] Z. Dworakowski, P. Kohut, A. Gallina, K. Holak, and T. Uhl, "Vision-based algorithms for damage detection and localization in structural health monitoring," *Struct. Control Health Monitor.*, vol. 23, no. 1, pp. 35–50, Jan. 2016.
[10] L. J. Dong, J. Wesseloo, Y. Potvin, and X. B. Li, "Discriminant models of blasts and seismic events in mine seismology," *Int. J. Rock Mech. Mining Sci.*, vol. 86, pp. 282–291, Jul. 2016.
[11] L. Dong, J. Wesseloo, Y. Potvin, and X. Li, "Discrimination of mine seismic events and blasts using the fisher classifier, naive Bayesian classifier and logistic regression," *Rock Mech. Rock Eng.*, vol. 49, no. 1, pp. 183–211, Jan. 2016.
[12] J. He and F.-G. Yuan, "Damage identification for composite structures using a cross-correlation reverse-time migration technique," *Struct. Health Monitor.*, vol. 14, no. 6, pp. 558–570, Sep. 2015.
[13] L. Dong, D. Sun, X. Li, and K. Du, "Theoretical and experimental studies of localization methodology for AE and microseismic sources without pre-measured wave velocity in mines," *IEEE Access*, vol. 5, pp. 16818–16828, Aug. 2017.
[14] L. Dong, W. Shu, G. Han, X. Li, and J. Wang, "A multi-step source localization method with narrowing velocity interval of cyber-physical systems in buildings," *IEEE Access*, vol. 5, pp. 20207–20219, Sep. 2017.
[15] C. Q. G. Muñoz and F. P. G. Márquez, "A new fault location approach for acoustic emission techniques in wind turbines," *Energies*, vol. 9, no. 1, p. 40, Jan. 2016.
[16] A. Ebrahimkhanlou and S. Salamone, "Acoustic emission source localization in thin metallic plates: A single-sensor approach based on multimodal edge reflections," *Ultrasonics*, vol. 78, pp. 134–145, Jul. 2017.
[17] W. Meng, L. Xie, and W. Xiao, "Optimal TDOA sensor-pair placement with uncertainty in source location," *IEEE Trans. Veh. Technol.*, vol. 65, no. 11, pp. 9260–9271, Nov. 2016.
[18] J. Li, H. Pang, F. Guo, L. Yang, and W. Jiang, "Localization of multiple disjoint sources with prior knowledge on source locations in the presence of sensor location errors," *Digit. Signal Process.*, vol. 40, pp. 181–197, May 2015.
[19] M. Ge, "Analysis of source location algorithms part I: Overview and non-iterative methods," *J. Acoust. Emiss.*, vol. 21, no. 1, pp. 14–24, 2003.
[20] M. Ge, "Analysis of source location algorithms part II: Iterative methods," *J. Acoust. Emiss.*, vol. 21, no. 1, pp. 29–51, Jan. 2003.
[21] L. Yang and K. C. Ho, "An approximately efficient TDOA localization algorithm in closed-form for locating multiple disjoint sources with erroneous sensor positions," *IEEE Trans. Signal Process.*, vol. 57, no. 12, pp. 4598–4615, Dec. 2009.
[22] L. Dong, X. Li, and G. Xie, "An analytical solution for acoustic emission source location for known P wave velocity system," *Math. Problems Eng.*, vol. 2014, Mar. 2014, Art. no. 290686.
[23] L.-J. Dong, X.-B. Li, Z.-L. Zhou, G.-H. Chen, and M. A. Ju, "Three-dimensional analytical solution of acoustic emission source location for cuboid monitoring network without pre-measured wave velocity," *Trans. Nonferrous Metals Soc. China*, vol. 25, no. 1, pp. 293–302, Jan. 2015.
[24] L. Dong, W. Shu, X. Li, G. Han, and W. Zou, "Three dimensional comprehensive analytical solutions for locating sources of sensor networks in unknown velocity mining system," *IEEE Access*, vol. 5, pp. 11337–11351, May 2017.
[25] L. Geiger, "Herdbestimmung bei erdbeben aus den ankunftszeiten," *Nachrichten Koninglichen Gesellschaft Wissenschaften Göttingen Math. Phys. Klasse*, vol. 4, pp. 331–349, Jan. 1910.
[26] C. H. Thurber, "Nonlinear earthquake location: Theory and examples," *Bull. Seismol. Soc. Amer.*, vol. 75, no. 3, pp. 779–790, Jun. 1985.
[27] B. R. Lienert, E. Berg, and L. N. Frazer, "HYPOCENTER: An earthquake location method using centered, scaled, and adaptively damped least squares," *Bull. Seismol. Soc. Amer.*, vol. 76, no. 3, pp. 771–783, Jun. 1986.
[28] L. J. Dong, X. B. Li, L.-Z. Tang, and F. Q. Gong, "Mathematical functions and parameters for microseismic source location without pre-measuring speed," *Chin. J. Rock Mech. Eng.*, vol. 30, no. 10, pp. 2057–2067, Oct. 2011.
[29] T. Kundu, "Acoustic source localization," *Ultrasonics*, vol. 54, no. 1, pp. 25–38, Jan. 2014.
[30] S. Sengupta, A. K. Datta, and P. Topdar, "Structural damage localisation by acoustic emission technique: A state of the art review," *Latin Amer. J. Solids Struct.*, vol. 12, no. 8, pp. 1565–1582, Aug. 2015.
[31] G. L. Feng, X. T. Feng, B. R. Chen, Y. X. Xiao, and Q. Jiang, "Sectional velocity model for microseismic source location in tunnels," *Tunnelling Underground Space Technol.*, vol. 45, pp. 73–83, Jan. 2015.
[32] S. Kalafat and M. G. R. Sause, "Acoustic emission source localization by artificial neural networks," *Struct. Health Monitor.*, vol. 14, no. 6, pp. 633–647, Oct. 2015.
[33] T. Kundu, X. Yang, H. Nakatani, and N. Takeda, "A two-step hybrid technique for accurately localizing acoustic source in anisotropic structures without knowing their material properties," *Ultrasonics*, vol. 56, pp. 271–278, Feb. 2015.
[34] J. P. Mccrory *et al.*, "Damage classification in carbon fibre composites using acoustic emission: A comparison of three techniques," *Compos. B, Eng.*, vol. 68, no. 5, pp. 424–430, Jan. 2015.
[35] E. D. Niri, A. Farhidzadeh, and S. Salamone, "Determination of the probability zone for acoustic emission source location in cylindrical shell structures," *Mech. Syst. Signal Process.*, vol. 60, pp. 971–985, Aug. 2015.
[36] J. Li and G. Qi, "Improving source location accuracy of acoustic emission in complicated structures," *J. Nondestruct. Eval.*, vol. 28, no. 1, pp. 1–8, Mar. 2009.
[37] J. Zhang, "Effects of anisotropy for P-wave velocity on locating accuracy of acoustic emission sources in sandstone," *IEEE Access*, vol. 5, pp. 18132–18142, Aug. 2017.
[38] S. Gollob, G. K. Kocur, T. Schumacher, L. Mhamdi, and T. Vogel, "A novel multi-segment path analysis based on a heterogeneous velocity model for the localization of acoustic emission sources in complex propagation media," *Ultrasonics*, vol. 74, pp. 48–61, Feb. 2017.
[39] G. Prasanna, M. R. Bhat, and C. R. L. Murthy, "Acoustic emission source location on an arbitrary surface by geodesic curve evolution," *J. Acoust. Emiss.*, vol. 25, pp. 224–230, Jan. 2007.
[40] R. Kiri, N. Quieffin, S. Catheline, and M. Fink, "In solid localization of finger impacts using acoustic time-reversal process," *Appl. Phys. Lett.*, vol. 87, no. 20, p. 204104, 2005.
[41] G. Ribay, S. Catheline, D. Clorennec, R. K. Ing, N. Quieffin, and M. Fink, "Acoustic impact localization in plates: Properties and stability to temperature variation," *IEEE Trans. Ultrason., Ferroelect., Freq. Control*, vol. 54, no. 2, pp. 378–385, Feb. 2007.
[42] B. Park, H. Sohn, S. E. Olson, M. P. DeSimio, K. S. Brown, and M. M. Derriso, "Impact localization in complex structures using laser-based time reversal," *Struct. Health Monitor.*, vol. 11, no. 5, pp. 577–588, Sep. 2012.
[43] M. G. Baxter, R. Pullin, K. M. Holford, and S. L. Evans, "Delta *T* source location for acoustic emission," *Mech. Syst. Signal Process.*, vol. 21, no. 3, pp. 1512–1520, Apr. 2007.
[44] J. Hensman, R. Mills, S. G. Pierce, K. Worden, and M. Eaton, "Locating acoustic emission sources in complex structures using Gaussian processes," *Mech. Syst. Signal Process.*, vol. 24, no. 1, pp. 211–223, Jan. 2010.
[45] M. J. Eaton, R. Pullin, and K. M. Holford, "Acoustic emission source location in composite materials using Delta T mapping," *Compos. A, Appl. Sci. Manuf.*, vol. 43, no. 6, pp. 856–863, Jun. 2012.
[46] R. Ernst and J. Dual, "Acoustic emission localization in beams based on time reversed dispersion," *Ultrasonics*, vol. 54, no. 6, pp. 1522–1533, Aug. 2014.
[47] S. K. Al-Jumaili, M. R. Pearson, K. M. Holford, M. J. Eaton, and R. Pullin, "Acoustic emission source location in complex structures using full automatic delta T mapping technique," *Mech. Syst. Signal Process.*, vol. 72, pp. 513–524, May 2016.
[48] X. D. Zhang, S. Wang, B. Zhao, and H. Y. Jia, "Precise positioning in double-layer horizontal media," *Chin. J. Geotech. Eng.*, vol. 36, no. 6, pp. 1044–1050, Jun. 2014.
[49] X.-D. Zhang, S. Wang, and B.-X. Jia, "Positioning of seismic sources combined with forward and inversion of spherical wave in double-layer horizontal media," *Chin. J. Geotech. Eng.*, vol. 37, no. 2, pp. 225–234, Feb. 2015.

[50] Z.-L. Zhou, J. Zhou, L.-J. Dong, X. Cai, Y.-C. Rui, and C.-T. Ke, "Experimental study on the location of an acoustic emission source considering refraction in different media," *Sci. Rep.*, vol. 7, no. 1, Aug. 2017, Art. no. 7472.
[51] M. X. Zhang, G. L. Wang, and R. B. Wu, "Determination of refraction points between the interfaces of multiple media in GPR," *J. Civil Aviation Univ. Chin.*, vol. 20, no. 6, pp. 20–24, Dec. 2002.
[52] D. W. Marquardt, "An algorithm for least-squares estimation of nonlinear parameters," *J. Soc. Ind. Appl. Math.*, vol. 11, no. 2, pp. 431–441, 1963.

ZILONG ZHOU received the Ph.D. degree from Central South University, Changsha, China, in 2007. He became an Associate Professor in 2009. From 2011 to 2012, he was a Visiting Professor at Toronto University, Canada. He is currently a Professor and the Vice Dean with the School of Resources and Safety Engineering, Central South University. He is also the Principal Scientist of the National Basic Research Program of China, the Cheung Kong Young Scholar of Chinese Department of Education, and the Project Leader of the National Outstanding Youth Fund of China. He has authored over 100 papers published in academic journals. His current research interests include rock dynamics, rock burst monitoring and prevention, mine collapse mechanism, and disaster control.

Dr. Zhou is a member of the Rock Dynamic Commission of the International Society for Rock Mechanics and the Executive Member of the Chinese Society for Rock Mechanics and Engineering. He has served as the chair or co-chair for almost 10 conference/workshops and technical forums. He received the National Prize of Scientific and Technological Progress, the Provincial Prize of Natural Science, the Provincial Excellent Doctor Degree Dissertation, and three other ministerial level awards.

YICHAO RUI received the B.Sc. degree in mining engineering from Henan Polytechnic University, Jiaozuo, China, in 2016. He is currently pursuing the M.Sc. degree in geotechnical engineering with Central South University. His research interests include rock mechanics and the location method of AE sources.

JING ZHOU received the B.Sc. degree in city underground space engineering from Central South University, Changsha, China, in 2015, where she is currently pursuing the M.Sc. degree in geotechnical engineering. Her research interests include rock mechanics and the location method of AE sources.

LONGJUN DONG (M'16) received the Ph.D. degree from the School of Resources and Safety Engineering, Central South University, Changsha, China, in 2013. From 2012 to 2013, he was an Assistant Researcher with the Australia Center for Geomechanics, The University of Western Australia, Perth, Australia. His current research interests include computational methods in location and identification for shock sources, seismic signals, machine learning algorithms, and rock/mineral mechanics for mining science.

He is currently an Associate Professor with the School of Resources and Safety Engineering, Central South University. He is a member of ASCE and ISRM. He has served as a reviewer for over 30 journals. He was selected for the Young Elite Scientists Sponsorship Program by the China Association for Science and Technology. He is invited to serve as the Editorial Board Member for *Scientific Reports*, the *Internal Journal of Distributed Sensor Networks*, and *Shock and Vibration*.

XIN CAI received the M.Sc. degree in architectural and civil engineering from Central South University, Changsha, China, in 2017, where he is currently pursuing the Ph.D. degree in geotechnical engineering. His research interests include rock dynamics, infrared properties of rock materials, mechanics of rock under moisture condition, and microseismic/AE source locating method.